

Energy dependent growth of the nucleon and hydrodynamic initial conditions

Ulrich Heinz^{1,*} and J. Scott Moreland^{1,2}

¹*Department of Physics, The Ohio State University, Columbus, OH 43210, USA*

²*Institut für Theoretische Physik, Johann Wolfgang Goethe-Universität,
Max-von-Laue-Straße 1, D-60438 Frankfurt am Main, Germany*

(Dated: August 13, 2018)

Due to gluon saturation, the growth of the inelastic nucleon-nucleon cross section with increasing collision energy \sqrt{s} results in a broadening of the nucleon's density distribution in position space. This leads to a natural smoothing of the initial energy density distribution in the transverse plane of the matter created near midrapidity in heavy-ion collisions. We study this effect for fluctuating initial conditions generated with the Monte Carlo Kharzeev-Levin-Nardi (MC-KLN) model for Au+Au collisions at the Relativistic Heavy Ion Collider (RHIC) and the Large Hadron Collider (LHC). We argue that at the LHC viscous hydrodynamics is applicable at earlier times than at RHIC, not only because of the higher temperature but also since the length scale over which the initial pressure fluctuates increases with collision energy.

PACS numbers: 25.75.-q, 12.38.Mh, 25.75.Ld, 24.10.Nz

I. INTRODUCTION

Hydrodynamics has been successful in modeling the hot, dense matter produced in ultra-relativistic heavy-ion collisions, particularly in describing the large collective flow observed at RHIC and the LHC [1]. A fully quantitative description of the experimental data requires, among other ingredients, realistic initial conditions. These initial conditions currently remain a significant source of uncertainty in predicting final state observables.

Optical models [2–4] for the 2-dimensional initial density profile in the plane transverse to the beam axis, generated from the overlap of longitudinally integrated Woods-Saxon distributions (“nuclear thickness functions”), yield radially symmetric entropy and energy densities for zero impact parameter ($b=0$) collisions. This symmetry drives radially symmetric hydrodynamic expansion, with zero anisotropic flow coefficients $v_n \equiv \langle \cos(n\phi) \rangle$ (where ϕ is the azimuthal angle in the transverse plane relative to the impact parameter, and the average is taken with the azimuthal distribution of the final state particles). The non-vanishing elliptic flow v_2 observed in central ($b \approx 0$) Cu+Cu and Au+Au collisions at RHIC [5] and the non-zero harmonic flow coefficients v_1, \dots, v_6 measured in central Pb+Pb collisions at the LHC [6–8] are in direct conflict with this prediction and require new physics to model the density of matter produced in relativistic heavy-ion

collisions.

Collective flow is the hydrodynamical response to the pressure gradients in an individual collision event, and the latter fluctuate from event to event. In essence, each nuclear collision makes a quantum mechanical measurement of the actual transverse nucleon positions inside each nucleus at the time of collision, and the outcome of this measurement fluctuates stochastically even though the corresponding probability distribution (the average nuclear density profile) is smooth. Therefore, the initial density distribution of matter produced even in a perfectly central ($b=0$) collision is *not* azimuthally symmetric (and the resulting anisotropic flow coefficients v_n do *not* vanish) even though the ensemble-averaged initial density has this symmetry.

This was first pointed out by Miller and Snellings [9] who demonstrated the importance of event-by-event initial state fluctuations on anisotropic collective flow using a Monte Carlo implementation of the Glauber model [10]. A Monte Carlo version of the KLN model [4], which incorporates the idea of gluon saturation at high collision energies, was later developed by Drescher and Nara [11] and further improved in Refs. [12–14].

The original MC-KLN code [11, 12] modeled nucleons as homogeneous cylinders along the beam direction whose cross section is determined by the (energy dependent) inelastic nucleon-nucleon scattering cross section $\sigma_{\text{NN}}^{\text{inel}}$. This leads to step-function-like discontinuities in the nuclear thickness function $T_A(\mathbf{r}_\perp)$, which (through the gluon saturation momentum $Q_s^2(\mathbf{r}_\perp)$ [4]) controls the initial transverse entropy density profile $s(\mathbf{r}_\perp)$ of the collision fire-

*Correspond to heinz@mps.ohio-state.edu

ball [15]. These artificial discontinuities generate big fluctuations in the initial hydrodynamic velocity gradients which create such large viscous pressure gradients that viscous hydrodynamics breaks down. This can be avoided by using a more realistic Gaussian profile for the nucleon density [14]. In [14] it was assumed that small- x evolution is local in impact parameter space, which may underestimate the broadening of the dipole scattering amplitude in impact parameter space with increasing collision energy. We here point out that, if one follows the idea of gluon saturation, the width of the gluon distribution inside a nucleon should grow with energy, due to transverse diffusion of small- x gluons: as \sqrt{s} increases, both $\sigma_{\text{NN}}^{\text{inel}}$ and σ should become larger. We model this by an energy-dependent broadening of the Gaussian nucleon thickness function $T_p(\mathbf{r}_\perp)$.¹ We show that this broadening leads to a smoothing of fluctuations in the initial density distribution of higher-energy heavy-ion collisions and to a corresponding decrease of the higher order eccentricity coefficients $\varepsilon_{n>2}$ (which drive the higher order anisotropic flow coefficients $v_{n>2}$ [19]) at the LHC compared to RHIC.

II. SIZING THE NUCLEON

We consider Gaussian nucleons with the normalized density distribution (the subscript p stands for "proton")

$$\rho_p(\mathbf{r}) = \frac{e^{-r^2/(2B)}}{(2\pi B)^{3/2}}, \quad \left(\int d^3r \rho_p(\mathbf{r}) = 1\right), \quad (1)$$

corresponding to a 3-dimensional rms radius of the nucleon of $r_p^{\text{rms}} = \sqrt{\langle r^2 \rangle} = \sqrt{3B}$. Eq. (1) yields the nucleon thickness function (defined as the integral of the nucleon density along the beam axis)

$$T_p(\mathbf{r}_\perp) = \int dz \rho_p(\mathbf{r}_\perp, z) = \frac{e^{-r_\perp^2/(2B)}}{2\pi B},$$

$$\int d^2r_\perp T_p(\mathbf{r}_\perp) = 1, \quad (2)$$

¹ The possibility of measuring this broadening at a future electron-ion collider has recently been pointed out in Ref. [16]. We also note that similar ideas precede the development of the concept of gluon saturation and follow from Froissart's work on the unitarization of scattering amplitudes [17], see [18] for a review.

corresponding to a transverse rms radius $r_\perp^{\text{rms}} = \sqrt{2B}$. We interpret it as the longitudinally integrated ("transverse") density of colored partons ("gluons") inside the proton.

In this section, we determine the Gaussian width B as a function of \sqrt{s} by relating it to the \sqrt{s} -dependent inelastic nucleon-nucleon cross section $\sigma_{\text{NN}}^{\text{inel}}$. Motivated by the Glauber-Mueller formula for the impact parameter dependent cross section of a color dipole with the quarks and gluons inside a proton [20, 21], we make a Glauber-like ansatz [14] for the probability $P(b)$ of a nucleon-nucleon collision at impact parameter b :

$$P(b) = 1 - \exp[-\sigma_{gg} T_{pp}(b)]. \quad (3)$$

Here $T_{pp}(b)$ is the transverse density for binary collisions between gluons,

$$T_{pp}(b) = \int d^2r_\perp T_p(\mathbf{r}_\perp) T_p(\mathbf{b}-\mathbf{r}_\perp) = \frac{e^{-b^2/(4B)}}{4\pi B},$$

$$\int d^2b T_{pp}(b) = 1, \quad (4)$$

and σ_{gg} is the glue-gluon interaction cross section.

We are mostly interested in the initial transverse density distribution of the matter created at mid-rapidity in heavy-ion collisions. As the collision energy increases, the production processes for this matter involve gluons of smaller and smaller longitudinal momentum fraction x . As x decreases, the gluon density (gluon distribution function) grows [22]. At high gluon densities, gluons start to recombine [23], leading eventually to a saturation of the gluon density [24]. For a Gaussian density distribution as in Eq. (1) gluon saturation becomes effective in the center of the proton first, reaching into the periphery only at still higher collision energies. This leads to a flattening of the normalized density distribution (1) near its center, accompanied by a growth of its rms radius. Gluon saturation effects can therefore be mimicked by allowing the parameter B in Eq. (1) to grow with \sqrt{s} . This is what we suggest in the present article; it differs from the treatments in [14, 21] which held B constant.

The inelastic nucleon-nucleon cross section $\sigma_{\text{NN}}^{\text{inel}}$ is obtained by integrating the inelastic gluon-scattering probability $P(b)$ in Eq. (3) over all impact parameters:

$$\sigma_{\text{NN}}^{\text{inel}} = \int d^2b P(b) = \int d^2b \left(1 - \exp[-\sigma_{gg} T_{pp}(b)]\right). \quad (5)$$

In our model the \sqrt{s} dependence of $\sigma_{\text{NN}}^{\text{inel}}$ results from the combined energy dependences of σ_{gg} and the

Gaussian width B of $T_{pp}(b)$. This differs from the work [14] where the \sqrt{s} dependence of $\sigma_{\text{NN}}^{\text{inel}}$ arises entirely from the energy dependence of σ_{gg} .

With the explicit form (4) for the binary gluon collision density and the substitutions $t=b^2/(4B)$ and $\lambda=\sigma_{gg}/(4\pi B)$, relation (5) can be written as

$$\frac{\sigma_{\text{NN}}^{\text{inel}}}{4\pi B} = f(\lambda), \quad (6)$$

where

$$f(\lambda) = \int_0^\infty dt \left(1 - \exp(-\lambda e^{-t})\right) \quad (7)$$

is a monotonically increasing function with $f(0)=0$.

To completely specify our model we assume that $\lambda=\sigma_{gg}/(4\pi B)$ is an energy independent constant, or (equivalently) that the Gaussian width B (which is proportional to the square of the proton radius) increases with collision energy proportionally to the inelastic nucleon-nucleon cross section $\sigma_{\text{NN}}^{\text{inel}}$. This assumption makes intuitive sense: as the collision energy increases, we partons in the tail of the proton's density distribution get boosted to sufficient energy to contribute to the scattering between nucleons while a similar increase in the dense center of the proton gets tempered by gluon saturation. As a result, the proton gets bigger. The glue-gluon interaction cross section σ_{gg} increases at the same rate; in fact, since $P(b)$ is always smaller than 1 (due to the non-vanishing "punch-through" probability described by the last term in Eq. (3)), $\sigma_{gg} > \sigma_{\text{NN}}^{\text{inel}}$ is always true.²

To fix λ we use experimental input at fixed collision energy that is sufficiently large for the Glauber model [2] and our gluon-saturation-based ideas for extrapolating to higher energies to work, but small enough that we can still make contact with the measured and tabulated nuclear profiles at low energies, without having to take into account energy-dependent swelling of the entire nucleus.

At $\sqrt{s}=23.5$ GeV, the inelastic nucleon-nucleon cross section has been measured as $\sigma_{\text{NN}}^{\text{inel}}=3.2$ fm²

² There is no fundamental reason for assuming $\lambda = \sigma_{gg}/(4\pi B)$ to be constant. In fact, asymptotic freedom in QCD suggests that σ_{gg} might grow more slowly with \sqrt{s} than B , in which case λ and $f(\lambda)$ would be decreasing functions of \sqrt{s} , and the proton size B would grow more strongly with energy than the inelastic nucleon-nucleon cross section. This would further increase the smoothing effects on initial state fluctuations at higher collision energies to be discussed below.

[25]. An extraction of the rms impact parameter $b_{\text{rms}} = \langle b^2 \rangle^{1/2}$ for inelastic proton-proton collisions from CERN ISR data has been reported by Amaldi and Schubert [26]: at $\sqrt{s}=23.5$ GeV they find $b_{\text{rms}}=1.03$ fm. Our model allows to compute b_{rms} from the collision probability $P(b)$ in Eq. (3) as follows:

$$\begin{aligned} \langle b^2 \rangle &= \frac{\int d^2b b^2 P(b)}{\int d^2b P(b)} \\ &= 4B \frac{\int_0^\infty dt t (1 - \exp(-\lambda e^{-t}))}{\int_0^\infty dt (1 - \exp(-\lambda e^{-t}))} \equiv 4B g(\lambda). \end{aligned} \quad (8)$$

Equations (6) and (8) can be cast into the form

$$B = \frac{\sigma_{\text{NN}}^{\text{inel}}}{4\pi f(\lambda)} = \frac{\langle b^2 \rangle}{4g(\lambda)}, \quad (9)$$

which can be solved for both the energy-independent constant λ and the proton width parameter B at $\sqrt{s}=23.5$ GeV. We find $\lambda=1.62$, corresponding to $B(23.5 \text{ GeV})=(0.473 \text{ fm})^2$. At other collision energies B can now be computed from

$$B(\sqrt{s}) = \frac{\sigma_{\text{NN}}^{\text{inel}}(\sqrt{s})}{14.30 \text{ fm}^2}. \quad (10)$$

In Table I we collect a few representative values.

TABLE I: The Gaussian width \sqrt{B} (Eq. (10)) for various collision energies. The values for $\sigma_{\text{NN}}^{\text{inel}}$ at LHC energies (2.76 and 7 TeV) were reported in [28, 29].

\sqrt{s} (GeV)	$\sigma_{\text{NN}}^{\text{inel}}$ (mb)	\sqrt{B} (fm)
23.5	32	0.473
200	42	0.544
2760	62.1	0.661
7000	71	0.707

Before describing how we distribute these "growing nucleons" inside the colliding nuclei, let us summarize the novel features of our approach. In [14] all of the energy dependence of $\sigma_{\text{NN}}^{\text{inel}}$ on the l.h.s. of Eq. (5) was attributed to the factor σ_{gg} in the exponent on the r.h.s. of Eq. (5). Here we split this energy dependence between the factors σ_{gg} and $T_{pp}(b)$ on the r.h.s. of Eq. (5), by letting *both* σ_{gg} and the nucleon size B grow with \sqrt{s} . Our specific model assumption (for which we have no convincing argument other than simplicity) is that all three quantities ($\sigma_{\text{NN}}^{\text{inel}}$, σ_{gg} and B) grow at exactly the

same rate. While this may not be completely correct, *some* growth of the nucleon size B with \sqrt{s} is suggested by theory [30] and required by experimental data [26, 30, 31]: Amaldi and Schubert demonstrated a moderate growth of the proton *inelastic* interaction radius over the energy range probed by the ISR [26], and Fig. 19(E) in Ref. [30] together with the recent TOTEM result from elastic pp scattering at $\sqrt{s} = 7$ TeV at the LHC provide experimental evidence for a significant growth of the proton's *elastic* interaction radius by a factor ~ 2 between low ISR and top LHC energies, roughly comparable with the similar increase of $\sigma_{\text{NN}}^{\text{inel}}$ over the same energy range documented in Table I. It is this growth of the proton radius that causes the smearing of event-by-event fluctuations in very high energy nuclear collisions to be discussed in the following.

III. DISTRIBUTION OF NUCLEONS

To describe the two incoming nuclei before the collision, we distribute the nucleons (1) with a distribution $\tilde{\rho}_A(\mathbf{r}_0)$ (where \mathbf{r}_0 denotes the center of the nucleon) that is adjusted such that the resulting folded distribution [12]

$$\rho_A(\mathbf{r}) = \int d^3r_0 \tilde{\rho}_A(\mathbf{r}_0) \rho_p(\mathbf{r}-\mathbf{r}_0) \quad (11)$$

reproduces the measured nuclear density profile for a nucleus of mass number A [27]. We take both ρ_A and $\tilde{\rho}_A$ to be of Woods-Saxon form:

$$\rho_A(r) = \frac{\rho_0}{\exp\left(\frac{r-R_A}{d_A}\right) + 1}, \quad (12)$$

$$\tilde{\rho}_A(r_0) = \frac{\tilde{\rho}_0}{\exp\left(\frac{r_0-\tilde{R}_A}{\tilde{d}_A}\right) + 1}. \quad (13)$$

The measured values for gold are [12, 27]

$$\rho_0 = 0.1695 \text{ fm}^{-3}, \quad R_{\text{Au}} = 6.38 \text{ fm}, \quad d_{\text{Au}} = 0.535 \text{ fm}. \quad (14)$$

We find that the choice $\tilde{\rho}_0 = \rho_0$ works with excellent accuracy (see Fig. 1). We perform a two-parameter fit for \tilde{R}_{Au} and \tilde{d}_{Au} , using $\sqrt{B} = 0.473$ fm in Eq. (1) (*i.e.* the value corresponding to the lowest collision energy in Table I, keeping in mind that the parameters (14) are the result of low-energy scattering experiments). We thus find

$$\tilde{\rho}_0 = 0.1695 \text{ fm}^{-3}, \quad \tilde{R}_{\text{Au}} = 6.42 \text{ fm}, \quad \tilde{d}_{\text{Au}} = 0.45 \text{ fm}. \quad (15)$$

These values are very close to those obtained in [12] for a box-like nucleon density profile. Fig. 1 shows the nucleon center distribution $\tilde{\rho}_{\text{Au}}$ (Eq. (13)) and the folded distribution ρ_{Au} (Eq. (11)), and compares the latter to a Woods-Saxon profile (12) with the measured parameters (13).

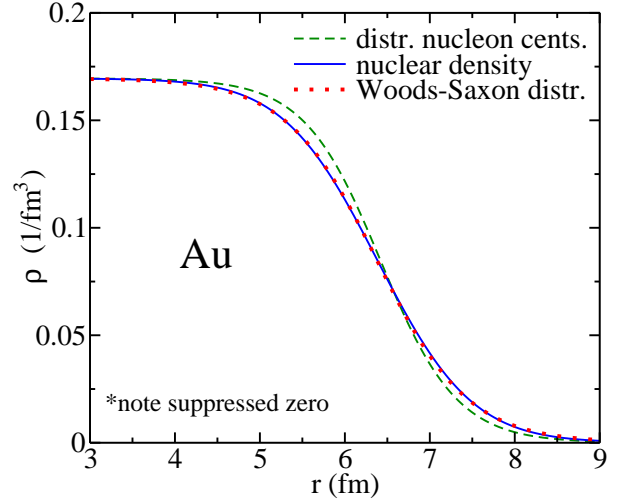


FIG. 1: (Color online) Nuclear density $\rho_{\text{Au}}(r)$ (Eq. (11), solid line) and the distribution of nucleon centers $\tilde{\rho}_{\text{Au}}(r)$ (Eqs. 12,14), dashed line), together with the Woods-Saxon distribution (12) with measured parameters (14) (dotted line). Please note that only the tail of the distribution is plotted, to better see the differences between $\rho_{\text{Au}}(r)$ and $\tilde{\rho}_{\text{Au}}(r)$.

IV. ENERGY DEPENDENCE OF INITIAL-STATE FLUCTUATIONS IN AU+AU COLLISIONS

The smooth dashed curve in Fig. 1 can be interpreted as the (unnormalized) probability (*i.e.* the squared modulus of the single-nucleon wave function) for finding a nucleon centered at position r inside a gold nucleus. At high energies, where the time for the colliding nuclei to pass through each other is very short, each nucleus-nucleus collision can be seen as performing an instantaneous position measurement of the positions of all struck nucleons inside the nuclei (*i.e.* of the A -particle wave function in position space, integrated over the positions of those nucleons that pass through unscathed). With few exceptions (see e.g. [32]), Monte Carlo implementations of these ideas assume uncorrelated nucleons (except for, in some cases, an excluded volume corresponding to an infinitely strong hard-core repulsion

at short distances), *i.e.* a factorization of the A -nucleon probability density into single-nucleon probabilities, given by the normalized version of Eq. (13). This allows to calculate the probabilities for distributing the A nucleons inside each nucleus independently.

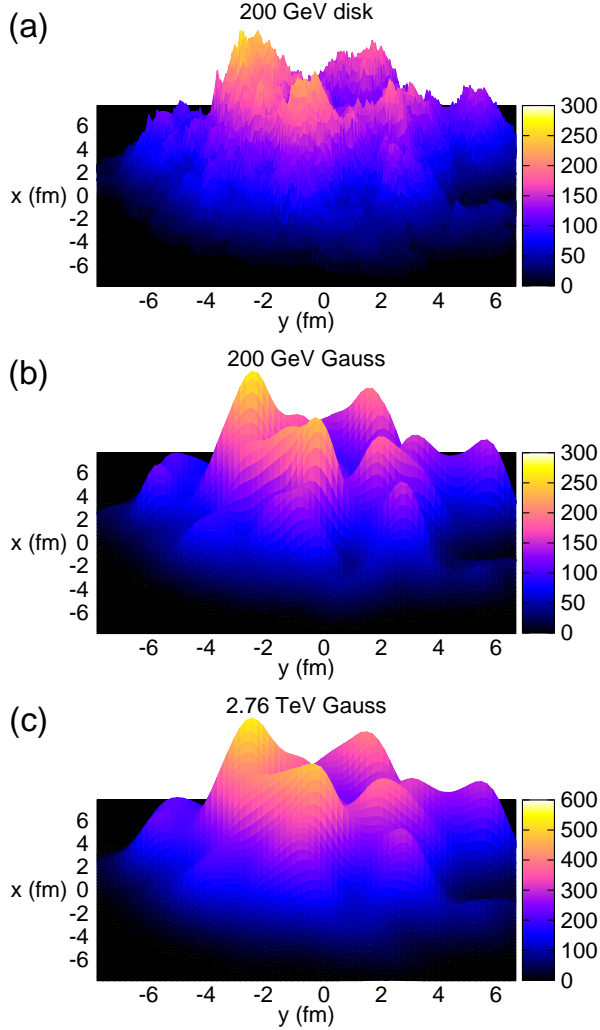


FIG. 2: (Color online) The transverse entropy density $s(\mathbf{r}_\perp, \tau_0 = 0.4 \text{ fm}/c)$ (in fm^{-3}) at mid-rapidity on an $8 \text{ fm} \times 8 \text{ fm}$ grid from the MC-KLN model, for a central ($b=0$) Au+Au collision. The top graph uses disk-like nucleons (Eq. (20) with $\sigma_{\text{NN}}^{\text{inel}} = 42 \text{ mb}$), whereas the middle and bottom plots use Gaussian nucleon thickness functions with $\sqrt{B} = 0.544$ and 0.707 fm , corresponding to collision energies of $\sqrt{s} = 200 \text{ GeV}$ and 7 TeV , respectively (see Table I). All three plots use the same collision event, *i.e.* identical spatial distributions for the nucleons in the two nuclei.

We here use the MC-KLN model described in

Ref. [11]. It calculates initial gluon production by folding the unintegrated gluon distributions of the two nuclei with a cross section for gluon fusion [33] (see Refs. [4, 11, 12, 15] for details). The unintegrated gluon distributions depend on transverse position through the gluon saturation momentum [11, 12]

$$Q_{s,A}^2(x, \mathbf{r}_\perp) = (2 \text{ GeV}^2) \left(\frac{T_A(\mathbf{r}_\perp)}{T_{A,0}} \right) \left(\frac{0.01}{x} \right)^\lambda, \quad (16)$$

where

$$T_A(\mathbf{r}_\perp) = \int dz \rho_A(\mathbf{r}_\perp, z) \quad (17)$$

is the nuclear thickness function of the corresponding nucleus at the same position, $T_{A,0} = 1.53 \text{ fm}^{-2}$, and $x = p_T \exp(\pm y)/\sqrt{s}$ are the longitudinal momentum fractions of the gluons from the two colliding nuclei that fuse into a produced gluon with rapidity y and transverse momentum p_T . The Monte Carlo sampling of the position distribution $\tilde{\rho}_A(\mathbf{r}_0)$ in Eq. (11) leads to event-by-event fluctuations in the nuclear thickness function $T_A(\mathbf{r}_\perp)$ that (via $Q_s^2(\mathbf{r}_\perp)$) are reflected in event-by-event fluctuations of the produced transverse gluon density which, after thermalization, generates the initial entropy and energy density profiles for the hydrodynamic evolution. Through Eq. (11), the shape and character of these fluctuations is affected by the nucleon density profile $\rho_p(r)$.

Integrating Eq. (11) over the longitudinal position z yields

$$T_A(\mathbf{r}_\perp) = \int d^2 r_{\perp 0} \tilde{T}_A(\mathbf{r}_{\perp 0}) T_p(\mathbf{r}_\perp - \mathbf{r}_{\perp 0}), \quad (18)$$

which, after distributing the nucleons in the nuclei by Monte Carlo sampling the distribution $\tilde{\rho}_A(\mathbf{r}_0)$, becomes

$$T_A(\mathbf{r}_\perp) = \sum_{i=1}^A T_p(|\mathbf{r}_\perp - \mathbf{r}_{i\perp}|). \quad (19)$$

Here the terms under the sum are Gaussians (2) with a width B that increases with \sqrt{s} as described in Sec. II. Previous implementations of the MC-KLN model [11, 12] instead used a disk-like nucleon thickness function:

$$T_p(r_\perp) = \frac{\theta(r_N - r_\perp)}{\sigma_{\text{NN}}^{\text{inel}}}, \quad r_N \equiv \sqrt{\frac{\sigma_{\text{NN}}^{\text{inel}}}{\pi}}. \quad (20)$$

In Figs. 2 and 3 we compare the initial transverse gluon density distributions for a central Au+Au collision with disk-like and Gaussian proton thickness

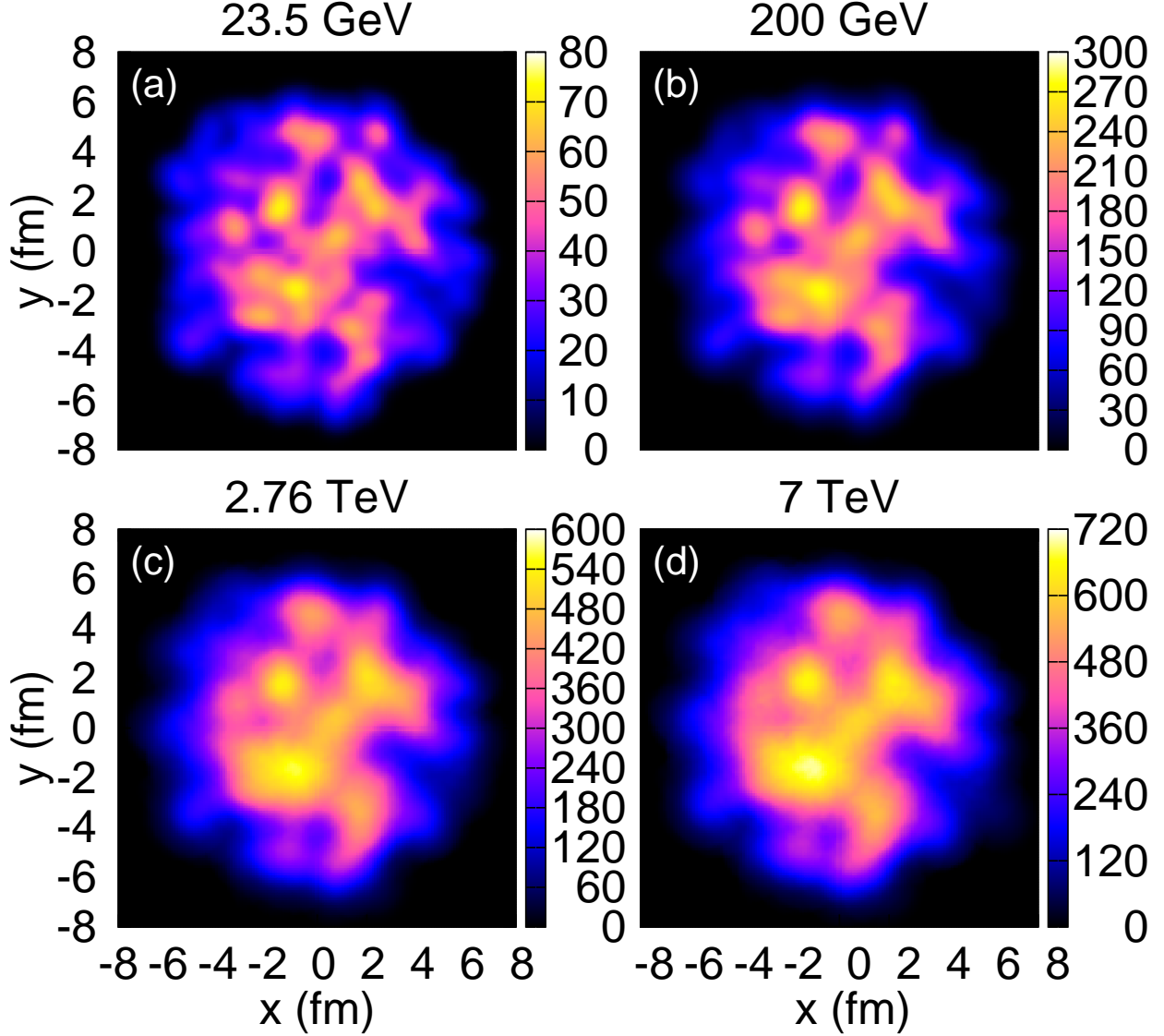


FIG. 3: (Color online) Influence of the growth of the proton with collision energy on the initial transverse entropy density $s(r_{\perp}, \tau_0 = 0.4 \text{ fm}/c)$ (in fm^{-3}) for a typical central ($b=0$) Au+Au collision from the MC-KLN model. All four panels use identical nucleon distributions in the two colliding nuclei, but the width \sqrt{B} of the nucleon thickness function changes with \sqrt{s} (indicated above each panel) as listed in Table I.

functions and for different collision energies, taking into account the growth of the width \sqrt{B} of the nucleon thickness function with increasing collision energy. The upper two panels in Fig. 2 illustrate the significant smoothing of the initial fireball density distribution at small length scales that is caused by replacing the disk-like nucleons with Gaussians. The small but pervasive discontinuities in the density profile using disk-like nucleons are unphysical but

constitute a major technical stumbling block for viscous hydrodynamics which cannot run stably with such discontinuous initial profiles (unless an additional smoothing step, involving another unphysical parameter, is applied first). With Gaussian nucleons these discontinuities are naturally washed out.

However, the initial density distributions shown in the middle panel of Fig. 2 and in the upper two panels of Fig. 3 still feature large (physical) inhom-

geneties and density gradients which, for very early starting times of the hydrodynamic evolution (where their effect on the viscous pressure is enhanced by a factor $1/\tau$ [34] that arises from the longitudinal Bjorken expansion), can drive viscous hydrodynamics outside its region of applicability. The length scale of these initial state density fluctuations thus generates a lower limit for the hydrodynamic starting time τ_0 . At earlier times, even if the system started out in a state of local equilibrium, viscous forces would drive the system so far away from thermal equilibrium that the macroscopic hydrodynamic framework breaks down.

The lower two panels in Fig. 2, as well as the profiles shown in Fig. 3, demonstrate that the growing nucleon size smoothes the initial state density fluctuations and significantly increases the length scale over which the initial pressure profile fluctuates. This implies that for heavy-ion collisions at the LHC viscous hydrodynamics can be applied starting from significantly earlier times than at RHIC energies.

V. FURTHER DISCUSSION AND CONCLUSIONS

The smoothing effects of a larger effective nucleon size at higher energies also influence the anisotropic flow generated in heavy ion collisions. Initial-state density fluctuations entail event-by-event shape fluctuations for the initially produced fireball. As discussed and studied in detail in Refs. [19, 35–37], these can be characterized by a set of harmonic eccentricity coefficients ε_n ($n=1, 2, \dots$) which drive higher order harmonic flow coefficients v_n .

Figure 4 shows the ratio of the ensemble averages $\langle \varepsilon_n \rangle$ of some of the first 15 harmonic eccentricity coefficients at two different energies. The ε_n are defined in terms of the initial transverse energy density profile $e(r_\perp, \phi)$ through [35, 38]

$$\varepsilon_n e^{in\psi_n} = - \frac{\int d^2r_\perp r_\perp^2 e^{in\phi} e(r_\perp, \phi)}{\int d^2r_\perp r_\perp^2 e(r_\perp, \phi)}. \quad (21)$$

Fig. 4 is for Au+Au collisions at RHIC and LHC energies as a function of collision centrality, using the MC-KLN model with Gaussian nucleons whose width grows with energy. We see that, except for the ellipticity ε_2 , all higher order harmonic eccentricity coefficients are larger at RHIC than at LHC, with the ratio between the two energies increasing with harmonic order n to about 1.5–1.6 for $n=15$. This is a straightforward reflection of the higher degree

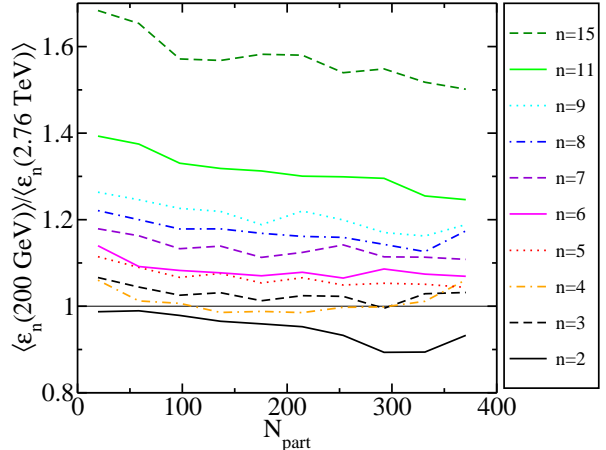


FIG. 4: (Color online) The ratio $\langle \varepsilon_n(200 \text{ GeV}) \rangle / \langle \varepsilon_n(2.76 \text{ TeV}) \rangle$ of the ensemble-averaged harmonic eccentricity coefficients $\langle \varepsilon_n \rangle$ ($n=2, \dots, 15$) at $\sqrt{s}=0.2$ and $2.76 A$ TeV, for Au+Au collisions with MC-KLN initial conditions as a function of the number of participating (struck) nucleons, N_{part} . The plot is based on 95,000 events, binned into 10 equal size N_{part} bins containing 9,500 events each. Smoother curves require higher statistics.

of granularity in the initial density profiles at RHIC than at LHC, caused by the smaller effective nucleon size. The ellipticity ε_2 bucks this trend: in contrast to the higher order harmonics which are driven by fluctuations, the ellipticity is dominated in all but the most central collisions by the elliptic geometric deformation of the nuclear overlap zone. The geometric contribution to the ellipticity actually *grows* with collision energy, due to the slight swelling of the entire nucleus caused by the growth of its constituent nucleons. Consequences for the extraction of the QGP shear viscosity from anisotropic flow coefficients will be explored in future work.

In summary, when taking into account the swelling of the nucleons at higher collision energy caused by gluon saturation effects, we expect the elliptic flow to slightly increase, but the higher order flow harmonics to decrease at the LHC compared to previous predictions. This effect increases with the harmonic order of the flow. Furthermore, smoother event-by-event initial conditions extend the range of validity of a viscous hydrodynamic description to earlier times, so taking into account the swelling of the nucleon from RHIC to LHC energies further adds to the applicability of viscous hydrodynamics for the description of the dynamical evolution of ultra-relativistic heavy-ion collisions.

Acknowledgments

We gratefully acknowledge clarifying discussions with Adrian Dumitru, Tetsu Hirano, Will Horowitz, Yuri Kovchegov, Mike Lisa, Yasushi Nara, Zhi Qiu, and Chun Shen, and thank Genya Levin for pointing us to Refs. [30, 31]. JSM wishes to thank Pasi Huovinen and Dirk Rischke and the Institute for Theoretical Physics at the J. W. Goethe Univer-

sität Frankfurt, where this work began, for their kind hospitality. The work of UH was supported by the U.S. Department of Energy under Grant No. DE-SC0004286. JSM received support from the ExtreMe Matter Institute (EMMI) and the BMBF under contract No. 06FY9092, and from the Undergraduate Research Office at The Ohio State University.

-
- [1] P. F. Kolb and U. Heinz, in *Quark-Gluon Plasma 3*, edited by R. C. Hwa and X. N. Wang (World Scientific, Singapore, 2004), p. 634 [nucl-th/0305084]; U. Heinz, in *Relativistic Heavy Ion Physics*, Landolt-Boernstein New Series, Vol. I/23, edited by R. Stock (Springer Verlag, New York, 2010), Chap. 5 [arXiv:0901.4355 [nucl-th]]; P. Romatschke, *Int. J. Mod. Phys. E* **19**, 1 (2010) D. A. Teaney, in *Quark-Gluon Plasma 4*, edited by R. C. Hwa and X. N. Wang (World Scientific, Singapore, 2010), p. 207 [arXiv:0905.2433 [nucl-th]].
- [2] R. J. Glauber, in *Lectures in Theoretical Physics*, edited by W. E. Brittin and L. G. Dunham (Interscience, N.Y., 1959), Vol. 1, p. 315.
- [3] P. F. Kolb, U. Heinz, P. Huovinen, K. J. Eskola, and K. Tuominen, *Nucl. Phys. A* **696**, 197 (2001).
- [4] D. Kharzeev and M. Nardi, *Phys. Lett. B* **507**, 121 (2001); D. Kharzeev and E. Levin, *Phys. Lett. B* **523**, 79 (2001); D. Kharzeev, E. Levin and M. Nardi, *Nucl. Phys. A* **747**, 609 (2005).
- [5] B. Alver *et al.* [PHOBOS Collaboration], *Phys. Rev. Lett.* **98**, 242302 (2007).
- [6] K. Aamodt *et al.* [ALICE Collaboration], *Phys. Rev. Lett.* **107**, 032301 (2011).
- [7] J. Velkovska *et al.* [CMS Collaboration], talk given at *Quark Matter 2011*, *J. Phys. G*, in press [<http://cdsweb.cern.ch/record/1366652>].
- [8] P. Steinberg *et al.* [ATLAS Collaboration], *J. Phys. G*, in press [arXiv:1107.2182 [nucl-ex]]; J. Jia *et al.* [ATLAS Collaboration], *J. Phys. G*, in press [arXiv:1107.1468 [nucl-ex]].
- [9] M. Miller and R. Snellings, arXiv:nucl-ex/0312008.
- [10] M. L. Miller, K. Reygers, S. J. Sanders and P. Steinberg, *Ann. Rev. Nucl. Part. Sci.* **57**, 205 (2007).
- [11] H. J. Drescher and Y. Nara, *Phys. Rev. C* **75**, 034905 (2007); *ibid.* **76**, 041903 (2007).
- [12] T. Hirano and Y. Nara, *Phys. Rev. C* **79**, 064904 (2009); and *Nucl. Phys. A* **830**, 191c (2009).
- [13] J. L. Albacete and A. Dumitru, arXiv:1011.5161 [hep-ph];
- [14] J. L. Albacete, A. Dumitru, and Y. Nara, arXiv:1106.0978 [nucl-th].
- [15] T. Hirano, U. Heinz, D. Kharzeev, R. Lacey and Y. Nara, *Phys. Lett. B* **636**, 299 (2006).
- [16] W. A. Horowitz, arXiv:1102.5058 [hep-ph].
- [17] M. Froissart, *Phys. Rev.* **123**, 1053 (1961).
- [18] A. Martin and G. Matthiae, in *Proton-Antiproton Collider Physics*, edited by G. Altarelli and L. Di Lella, Advanced Series on Directions in High Energy Physics, Vol. 4 (World Scientific, Singapore, 1989), p.45.
- [19] Z. Qiu and U. Heinz, *Phys. Rev. C* **84**, 024911 (2011) and arXiv:1108.1714 [nucl-th].
- [20] A. H. Mueller, *Nucl. Phys. B* **335**, 115 (1990).
- [21] H. Kowalski and D. Teaney, *Phys. Rev. D* **68**, 114005 (2003).
- [22] A. Deshpande, R. Milner, R. Venugopalan and W. Vogelsang, *Ann. Rev. Nucl. Part. Sci.* **55**, 165 (2005).
- [23] A. H. Mueller and J.-W. Qiu, *Nucl. Phys. B* **268**, 427 (1986).
- [24] J. Jalilian-Marian and Y. V. Kovchegov, *Prog. Part. Nucl. Phys.* **56**, 104 (2006).
- [25] K. Nakamura *et al.* [Particle Data Group Collaboration], *J. Phys. G* **37**, 075021 (2010).
- [26] U. Amaldi and K. R. Schubert, *Nucl. Phys. B* **166**, 301 (1980).
- [27] H. De Vries, C. W. De Jager and C. De Vries, *Atom. Data Nucl. Data Tabl.* **36**, 495 (1987).
- [28] A. Toia *et al.* [ALICE Collaboration], arXiv:1107.1973 [nucl-ex].
- [29] G. Aad *et al.* [ATLAS Collaboration], arXiv:1104.0326 [hep-ex].
- [30] E. Gotsman, E. Levin and U. Maor, *Eur. Phys. J. C* **71**, 1553 (2011).
- [31] G. Antchev *et al.* [TOTEM Collaboration], *Europhys. Lett.* **95**, 41001 (2011).
- [32] M. Alvioli, H.-J. Drescher and M. Strikman, *Phys. Lett. B* **680**, 225 (2009).
- [33] L. V. Gribov, E. M. Levin and M. G. Ryskin, *Phys. Rept.* **100**, 1 (1983).
- [34] D. Teaney, *Phys. Rev. C* **68**, 034913 (2003).
- [35] B. Alver and G. Roland, *Phys. Rev. C* **81**, 054905 (2010).
- [36] G.-Y. Qin, H. Petersen, S. A. Bass and B. Müller, *Phys. Rev. C* **82**, 064903 (2010).
- [37] R. S. Bhalerao, M. Luzum and J.-Y. Ollitrault, arXiv:1107.5485 [nucl-th].
- [38] B. H. Alver, C. Gombeaud, M. Luzum and J.-Y. Ollitrault, *Phys. Rev. C* **82**, 034913 (2010).